

## Dynamic Analysis and Optimization of a Bionic Flapping-Wing Aircraft

Xiaoyi JIN<sup>1)</sup>, Xiaolei ZHOU<sup>1)</sup>, Peipei TIAN<sup>1)</sup>,  
Liqiang ZHANG<sup>1)</sup>, Zhengwei NIE<sup>2)</sup>

<sup>1)</sup> *Shanghai University of Engineering Science  
Mechanical Design Department  
Mechanical Engineering College*

P.O. Box: 201620, Shanghai, China  
e-mail: jinxy@sues.edu.cn

<sup>2)</sup> *University of Missouri  
Department of Mechanical and Aerospace Engineering  
Columbia, MO 65211 USA*

This research has been conducted for the purpose of developing bionic flapping-wing aircraft. In this paper, wings are regarded as flexible, and the response issues of wings under certain excitation functions are investigated. The research is based on preliminary studies about bionic flapping wings and aims to provide data references to aid the selection of electrical actuators and the design of driving mechanisms for bionic flapping-wing aircraft at a later stage. The dynamic analysis shows that the response functions adapt well to the flapping movements of the wings. However, there are mutational situations in the wing structure transformation which are bad for structural stability, and cause there to be too little lift force. Under such circumstances, the minimum norm of low-order vibration mode difference values is used as the optimization principle to conduct the structural optimization. The optimization results and the wing flutter test both show that the optimized wings can better avoid structural mutations and their response functions can also better meet the design requirements.

**Key words:** bionic flapping-wing aircraft, flexible wings, structural mutation, structural optimization, flutter test.

### 1. INTRODUCTION

One of the future directions in the development of bionic flapping-wing aircraft is to make them small and portable, so that they can fly at a very low

height similar to insects. As it is found in nature, after millions of years of evolution, flapping-wing flight has many advantages in comparison to fixed-wing flight or rotor-wing flight. This type of flight allows for taking off, speeding up and hovering in the air. It has a very high manoeuvrability and flexibility [1, 2]. Many experts and researchers are now working on developing flapping wings.

To study and mimic insect or bird motion is to learn from the results of millions of years of evolution. MUELLER [3] and TIEN VAN TRUONG *et al.* [4] conducted a large number of experimental studies on the flow field and the aerodynamic performance of the wing flapping by using shock-wave velocity meter and hot-wire anemometry. Their studies involved the effects of backflows on boundary layer thickness and laminar-flow separation positions and the effects of turbulence and sound-wave stimulation on nonlinear lifting and hysteresis effects. However, due to the low Reynolds number, the condition, size and accuracy of the model used in the studies, wind tunnel turbulivity, the aerodynamic force measuring technology and data uncertainty resulted in big differences between the testing data collected by different wind tunnel devices. ZHENG *et al.* [5] conducted an examination in 2010 using a high-speed camera to observe free flying insects. The data collected were used as references for further stimulation calculation. YOUNG *et al.* [6] conducted a refined computational fluid mechanic stimulation of the real wing movement of locusts in 2008. They pointed out that the bending and torsion of wings can enhance the aerodynamic performance and lower the energy consumption.

This paper aims to further analyze a bionic flapping-wing aircraft that has already been designed. Through vibration analysis, the frequency features and dynamics generated in all parts of the flapping wings are calculated according to predetermined excitation functions; in addition, motion rules can be acquired. These calculations help to determine how the wing structure can be optimized and they offer a theoretical basis for further analysis of the aircraft dynamics and the design of the driving mechanism.

The study of bionic flapping-wing aircraft concerns wing transformations and morphologic changes that occur during the flapping. It is undoubtedly very hard to cover every aspect of this. In fact, a vein is an important part of an insect's wing. The vein offers primary rigidity and partial flexibility to the wing. Additionally, the vein contributes to 90% of the weight of the wing, while the membrane makes up only 10% [7]. Therefore, in this paper, analysis of the structural dynamics of the bionic flapping-wing aircraft will focus on analysis of the vein structure of the wing.

The wing structure used in our study, which was designed previously based on the theoretical bionics and size rule is shown in Fig. 1.

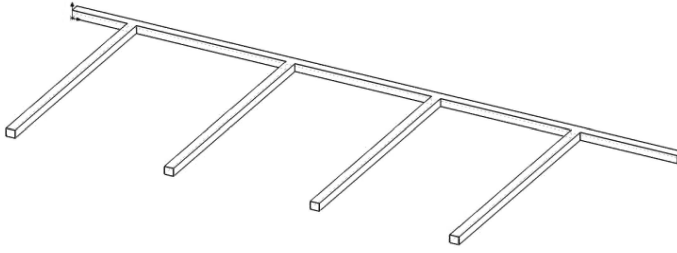


FIG. 1. Structural model of wing.

## 2. DYNAMIC ANALYSIS OF THE FLAPPING-WING STRUCTURE

### 2.1. Establishing the finite element model

While conducting analysis of a structural system,  $M$ ,  $C$  and  $K$  are usually used to represent the  $n$ -order positive definite mass matrix, the damping matrix and the stiffness matrix respectively. In addition,  $x(t)$ ,  $\dot{x}(t)$ ,  $\ddot{x}(t)$ ,  $p(t)$  represent the displacement, speed, acceleration and stimulation array of the structural system respectively. The equation of motion of the system can be indicated as [8]

$$M\ddot{x}(t) + C\dot{x}(t) + Kx(t) = p(t).$$

If  $w$  is the Fourier variable, after Fourier transform is conducted on the equation, there will be

$$\dot{X} = jwX, \quad \ddot{X} = -w^2X,$$

then

$$(2.1) \quad (K - w^2M + jwC)X(w) = P(w).$$

After the wing structure is simplified into a spatially rigid frame unit, a Timoshenko beam model will be assumed and analyzed. As a three-dimensional unit structure, this beam model is mainly affected by axial force, bending moment and torsion. Under micro transformative conditions, the characteristic matrix is constituted by the characteristic matrixes of the axial force unit, bending unit and the torsion unit [9].

The finite element model of the wing structure is simulated as shown in Fig. 2 by using a spatially rigid frame unit.

As is shown in the Fig. 2, the structure has 22 pitch points and 21 beam units (1 boundary support beam unit, 4 boundary non-support beam units and 16 central transition beam units).

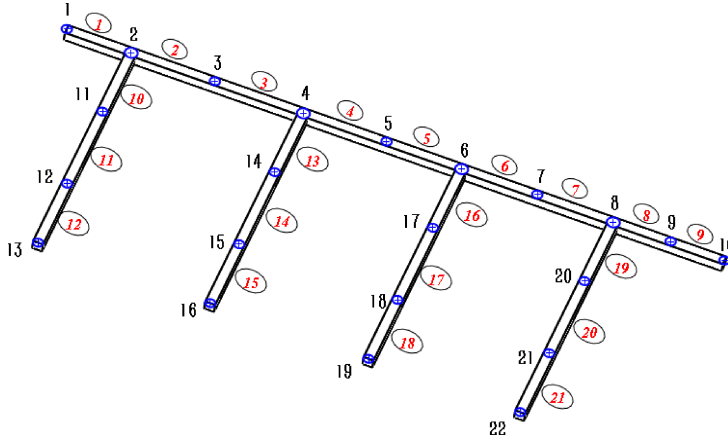


FIG. 2. Finite element structural model.

After selecting a beam unit from all the divided units, a local coordinate system of the double-pitch point unit is established first [10] (see Fig. 3).

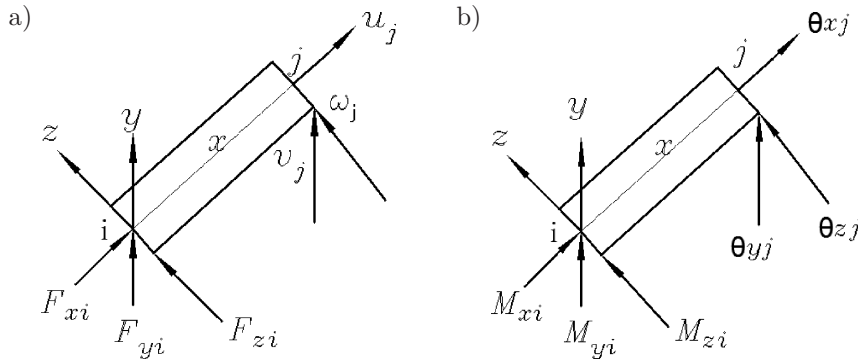


FIG. 3. Local coordinate systems: a) force and linear displacements, b) moment of force and cross-section rotations.

Use Timoshenko beams as the bending units. In terms of the spatially rigid frame unit, the relationship map of the local coordinate systems and the overall coordinate systems is demonstrated in Fig. 4.

In this research of wing structure, damping is hard to be confirmed since its value is located within a small scope. Thus, to simplify the calculation model, Rayleigh damping is adopted, which is the linear combination of the structure's overall mass matrix and rigidity matrix:

$$C = \alpha M + \beta K.$$

In the equation above,  $\alpha$  and  $\beta$  are two constants that are independent from the frequency.

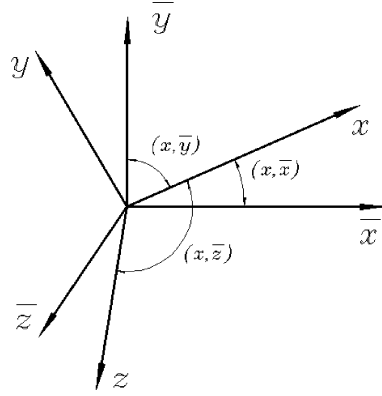


FIG. 4. Transforming relationship of coordinate systems.

The relationship between the Rayleigh damping matrix and the diagonal matrix  $\varphi_j^T C \varphi_i$  is

$$\varphi_j^T C \varphi_i = \begin{cases} c_i & i = j, \\ 0 & i \neq j. \end{cases}$$

On the basis of the Fourier transform, mass matrix, rigidity matrix and damping matrix, the displacement response of the system can be expressed as

$$(2.2) \quad X(w) = \sum_{i=1}^n \frac{\varphi_i \varphi_i^T P}{k_i - w^2 m_i + j w c_i}.$$

In the equation above,  $k_i = \varphi_i^T K \varphi_i$ ;  $m_i = \varphi_i^T M \varphi_i$ ;  $c_i = \varphi_i^T C \varphi_i$ .

The inherent frequency  $\lambda_i$  of the designed wing, the relevant vibration mode  $\varphi_i$  and the response function  $X(w)$  model have been completely established. The inherent frequency is  $\lambda_i = w_i^2$ , ( $i = 1, 2, \dots, n$ ), the relevant vibration mode  $\varphi_i$  is calculated using Eq. (1) and the response function  $X(w)$  is calculated using Eq. (2).

## 2.2. Solution of the finite element model

The motion model and the stimulation function are derived from the measurement results of an insect's free flight. The boundary condition of the insect's (bee) movements is the root segment that does not have any translation displacements and it only reciprocates flapping around the dead  $y$  axle. The motion rule of the flapping of the wing's root segment adopts the fitting data [11] of insect wing fit by fourth-order Fourier level ( $n = 4$ ):

$$P(t) = a_0 + \sum_{i=1}^n (a_i \cos(i \cdot k \cdot t) + b_i \sin(i \cdot k \cdot t)).$$

In the equation above,  $k$  is the reduced frequency and its parameters are listed in Table 1.

**Table 1.** Parameters of the stimulation function.

Parameters	Sizes	Parameters	Sizes
$a_0$	31.40611	$b_1$	11.83419
$a_1$	-57.31259	$b_2$	3.37326
$a_2$	11.60773	$b_3$	1.75002
$a_3$	-1.18904	$b_4$	0.37691
$a_4$	-0.13234	$k$	0.926

The map of the stimulation function of the wing is in Fig. 5.

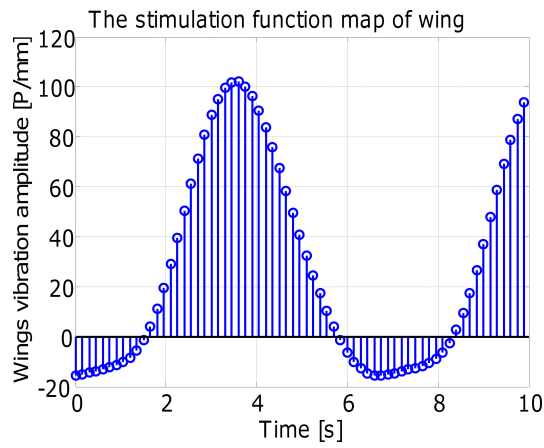


**FIG. 5.** Map of stimulation function of the wing.

The material used in this research is nylon 101 and its main attributes are shown in Table 2.

**Table 2.** Attributes of material.

Attribute	Value	Unit
Elasticity modulus	$1 \cdot 10^9$	$\text{N/m}^2$
Poisson ratio	0.3	None
Mass density	1150	$\text{kg/m}^3$
Tension strength	79289709	$\text{N/m}^2$
Yield force	$6 \cdot 10^7$	$\text{N/m}^2$

Modals contribute to the wing responses differently. The weight factors are in direct proportion to the reciprocals of the modal frequencies [12]. This means

that the features of low-order modals to some degree determine the dynamic property of wings. For a flapping-wing structure of flapping movement, the influence of high-order modals is much smaller than that of low-order modals. Therefore, low-order modals will be focused on in this research. Even though some errors will be generated, the amount of work will be significantly decreased as the matrix order of response function will be decreased as well. In fact, high-order modals basically will not appear in this paper due to the limitations of the flapping frequency of bionic flapping-wing aircraft [13]. Therefore, use modal truncation, and taking the first 5 order modes into consideration, that is,  $n = 5$ .

In this paper, it is therefore important to determine  $\lambda_i = w_i^2$ ,  $\varphi_i$ ,  $i = 1, 2, \dots, 5$ , and

$$X(w) = \sum_{i=1}^5 \frac{\varphi_i \varphi_i^T P}{k_i - w^2 m_i + j w c_i}.$$

The response results of the first five orders of the structure are calculated as shown in Fig. 6.

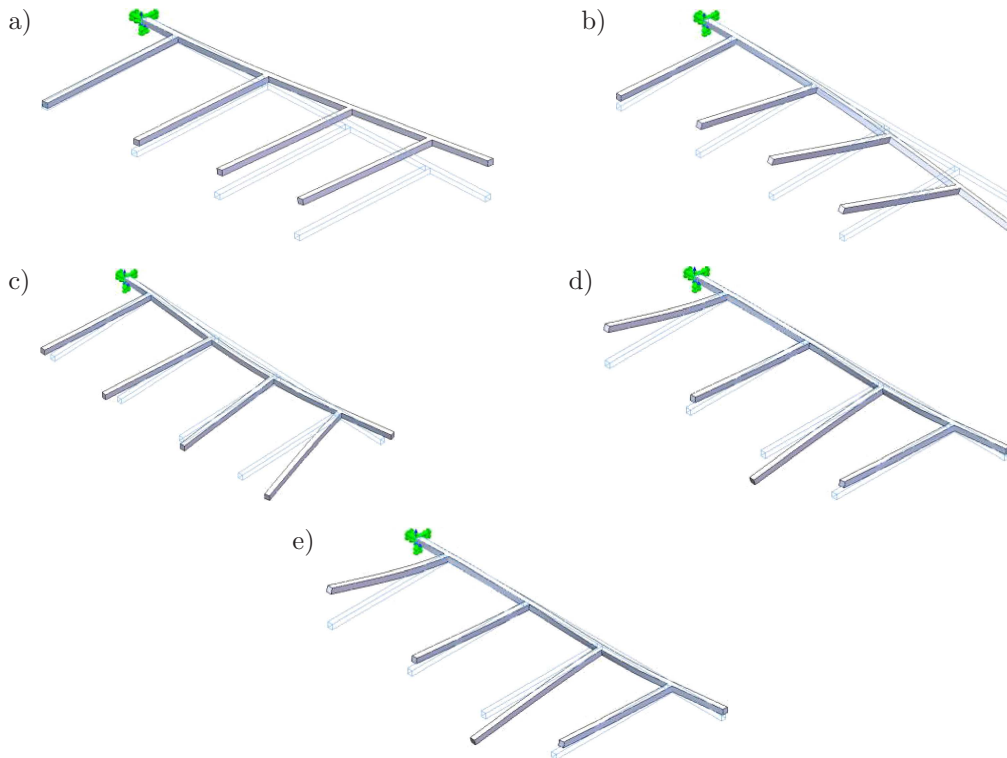


FIG. 6. Response results of the first five orders of modals: a) first-order, b) second-order, c) third-order, d) fourth-order, e) fifth-order.

The results of analysis of these modal responses are shown in Table 3.

**Table 3.** Modal analysis of wing structure.

Orders	Frequency [Hz]	Vibration modes
1	14.408	Main wing vein swinging, first-order bending vibration
2	40.941	Wing tendon vein sloping upwards, second-order bending vibration
3	64.546	Main wing vein transforming into the shape of saddle, third-order bending
4	99.814	Wing tendon veins intersecting and sloping upwards and downwards, first-order torsion vibration
5	112.170	Wing tendon veins intersecting reversely and sloping upwards and downwards, second-order torsion vibration

From the analysis above it can be seen that the inherent frequencies of the wing increase as the orders of the analyzed modals increase. The first three orders are main wing vein swinging, wing tendon veins sloping upwards and main wing vein transforming into the shape of saddle. The reasons for this are that the wing's integral rigidity is not enough and the shake-proof ability is weak which therefore needs to be improved. The fourth and fifth orders are the torsion and transformations of the wing tendon veins.

Figure 7 is the response map of the fifth-order modals of the wing structure's four transverse beams. And it is clear that they intersect positively and negatively.

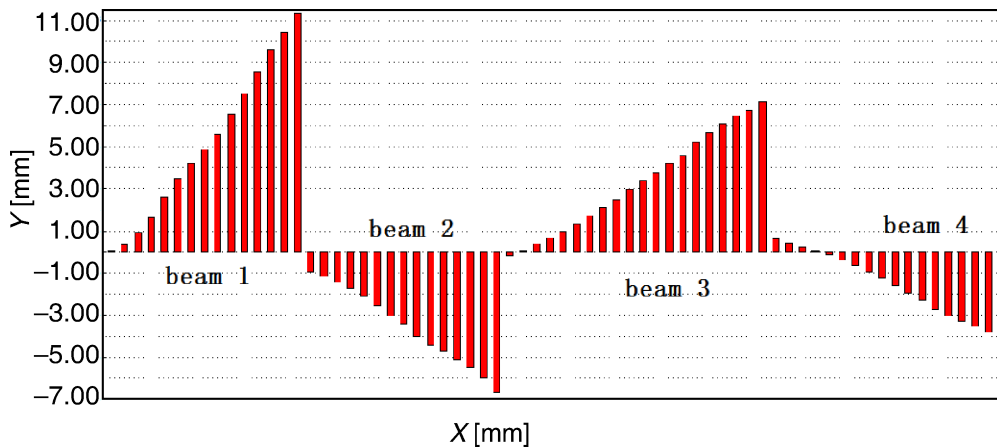


FIG. 7. Response map of boundary rectangular coordinates of the wing structure.

In order to better observe the intersections, a polar diagram is depicted below:

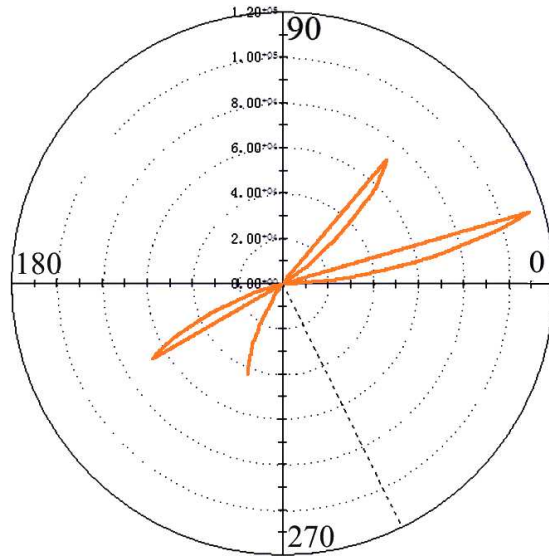


FIG. 8. Response map of boundary polar diagram of the wing structure.

From Fig. 8 it can be clearly seen that there are three mutational points. This indicates that the wings will easily transform (especially when the wings flap resonantly) during the flight of the bionic flapping-wing aircraft. If the wings fail to transform smoothly, the flight will not be able to be stable. This was why the previously designed aircraft designed vacillated to the left and right.

### 3. OPTIMIZATION DESIGN OF FLAPPING WINGS

Equation (2.1) tells us that if the conditions of designed stimulation function remain unchanged and the finite element models are similar, the inherent frequencies and relevant vibration modes and requirements of the original designed structures need to be alike to make their displacement amplitudes and stimulation responses similar.

It is hard to make the  $n$ -order frequencies and the relevant  $n$ -order vibration modes the same while designing the optimization from the perspective of dynamics [14]. From the perspective of the service conditions of bionic flapping-wing aircraft, the following optimization principles are worth considering: the inherent frequencies of the first  $N$  ( $N = 5$ ) orders satisfy the design requirements and the vibration modes of low-order (mainly the first-order) structures are close. This ensures the improvements of the structural low-order dynamic

responses, and provides that the low-order dynamic responses and the dynamic responses of original structure are nearly the same.

### 3.1. Establishment of optimization model

According to the previous analysis, the following optimization model is established.

In the research of wing-structure design, if only low-order dynamic feature indexes are taken into consideration, then

$$\begin{aligned} (K_A^0 + K_B^0)\Phi^0 &= (M_A^0 + M_B^0)\Phi^0 \Lambda^0, \\ \Phi_r^{0T}(K_A^0 + K_B^0)\Phi_r^0 &= \Lambda_r^0, \quad \Phi_r^{0T}(M_A^0 + M_B^0)\Phi_r^0 = E_r. \end{aligned}$$

In the equation,  $M_A^0$ ,  $K_A^0$  are the mass matrix and the rigidity matrix of the original structure; and  $M_B^0$ ,  $K_B^0$  are the mass matrix and the rigidity matrix of the optimized structure respectively, and  $\Lambda^0$ ,  $\Phi^0$  are respectively the inherent frequency and the vibration-mode matrix of the designed structure,

$$\Phi_r^0 = [\varphi_1^0 \ \varphi_2^0 \ \cdots \ \varphi_n^0] \Lambda_r^0 = \text{diag}(w_1^{02} \ w_2^{02} \ \cdots \ w_r^{02}), \quad r \leq n.$$

The mass matrix and the rigidity matrix of the structure are determined by the structural parameters  $b = [b_1 \ b_2 \ \dots \ b_n]$ . This means that the two matrices are functions of the structure's parameters which can be expressed as  $M_B^0(b)$ ,  $K_B^0(b)$ .

The selection of the limitation requirements is such that the inherent frequency needs to be close to the required frequency. So the minimum optimization principles of low-order vibration-mode difference values can be expressed using the following norms:

$$\begin{aligned} &\text{find } b, \\ \min \sum_j &\sqrt{\sum_i^n [\varphi_j(i) - \varphi_j^*(i)]^2}, \quad j = 1, 2, \dots, m, \\ \text{s.t. } g_r(b) &= |f_r - f_r^*| \leq \eta f_r^* (r = 1, 2, \dots, m), \\ &b_l \leq b \leq b_u. \end{aligned}$$

In the equation,  $\varphi_j$ ,  $f_r$  represent the vibration mode and the inherent frequency of the improved structure respectively;  $\varphi_j^*$ ,  $f_r^*$  represent the required vibration modes and the inherent frequency of the original wing-structure respectively;  $m$ ,  $N$  represent the vibration mode order and the order of frequency after the modal is being cut off and  $m \leq N$  (but here  $m = N$ );  $\eta$  represents the error-tolerate coefficient; and  $b_l$ ,  $b_u$  represent respectively the lower and upper limits of the conditional variables of the improved structure.

### 3.2. Planned optimization scheme

Considering that, in the scheme designed previously, the wing is unstable while in a flapping flight, the wing needs to be improved by adding a truss. Three possible optimized structures are presented in Fig. 9.

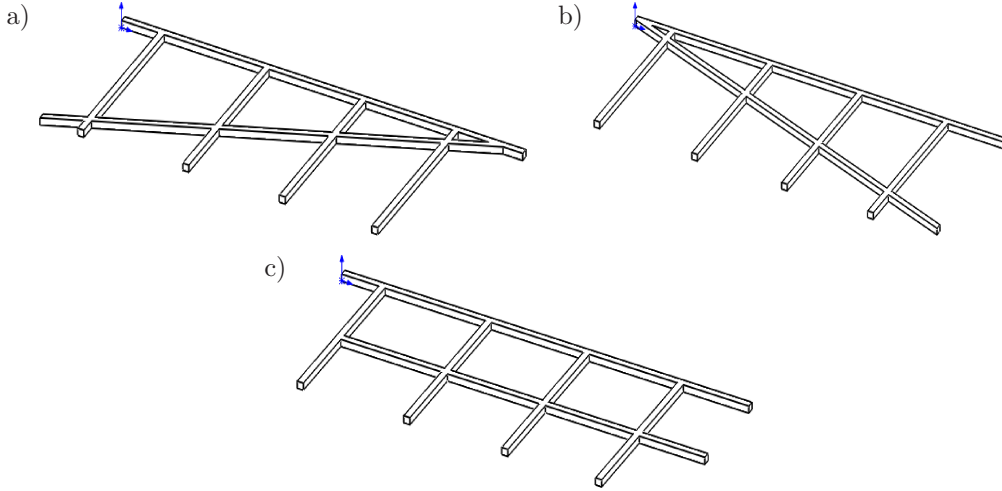


FIG. 9. Three optimized structure: a) structure 1, b) structure 2, c) structure 3.

### 3.3. Evaluation principles of optimization results

To better evaluate the three different schemes, the principle of modal assurance criterion (MAC) is adopted. This principle tests the extent of consistency of the vibration modes of the optimized structures and the original ones [15].

For random modal  $i$ , MAC can be expressed as

$$\text{MAC}_i = \frac{|\varphi_i^{*T} \varphi_i|^2}{(\varphi_i^{*T} \varphi_i^*)(\varphi_i^T \varphi_i)}.$$

In the equation,  $\varphi_i^*$  is the vibration mode of the original structure and  $\varphi_i$  is the vibration mode of the designed (optimized) structure. The equation tells us that the closer the MAC value is to 1, the better the extent of consistency of the vibration modes is.

### 3.4. Analysis of optimization results

To evaluate the schemes, MAC calculations are conducted for the three designed schemes and the original one. The results are listed in Table 4.

**Table 4.** Modal data of the wing-structures.

Orders		1	2	3	4	5
Original structure	frequency	14.4080	40.9410	64.5460	99.8140	112.1700
Optimized Structure 1	frequency	17.8100	76.1760	107.9400	132.5100	188.0400
	error	0.2361	0.8606	0.6723	0.3276	0.6764
	MAC	0.4313	0.7708	0.8581	0.4198	0.1726
Optimized Structure 2	frequency	16.3530	28.0650	52.9590	99.2440	136.5600
	error	0.1350	0.3145	0.1795	0.0057	0.2174
	MAC	0.9998	0.2137	0.0022	0.0405	0.4287
Optimized Structure 3	frequency	13.9060	48.9900	97.6400	141.8200	211.7600
	error	0.0348	0.1966	0.5127	0.4208	0.8878
	MAC	0.9956	0.8836	0.7671	0.6177	0.0233

The comparison maps of orders and MAC for different schemes are shown in Fig. 10 and Fig. 11.

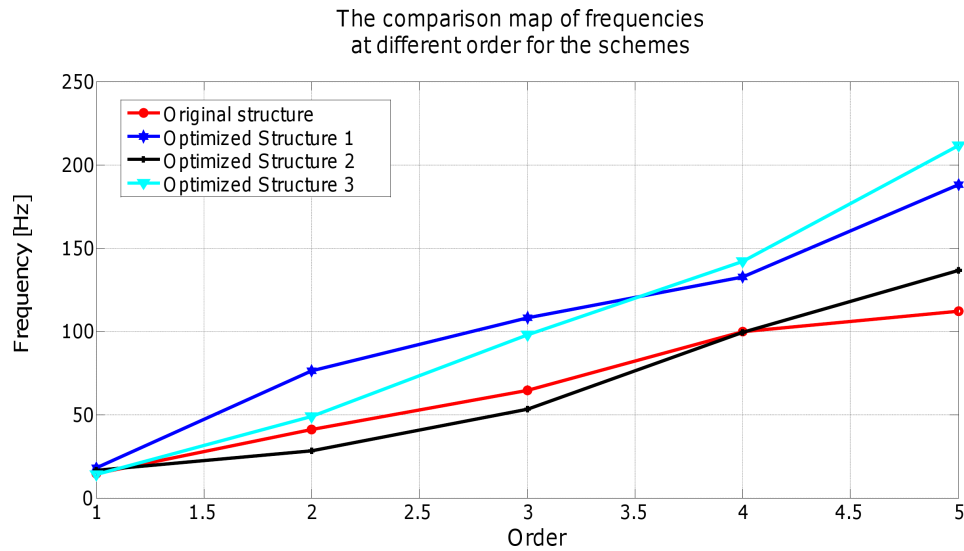


FIG. 10. Comparison map of frequencies at different orders for the schemes.

Table 4 and Fig. 10 show that optimized structure 2 is better because the frequency error is the smallest and its frequencies at the orders are the closest to the original scheme.

Table 4 and Fig. 11 demonstrate that among the first five modals, the MAC of optimized structure 3 is the most ideal and then that of optimized structure 1 and 2. In fact, according to bionic and size rule, the initial frequency of the bionic flapping-wing aircraft is 15 Hz. Taking the modal cutting off discussed before

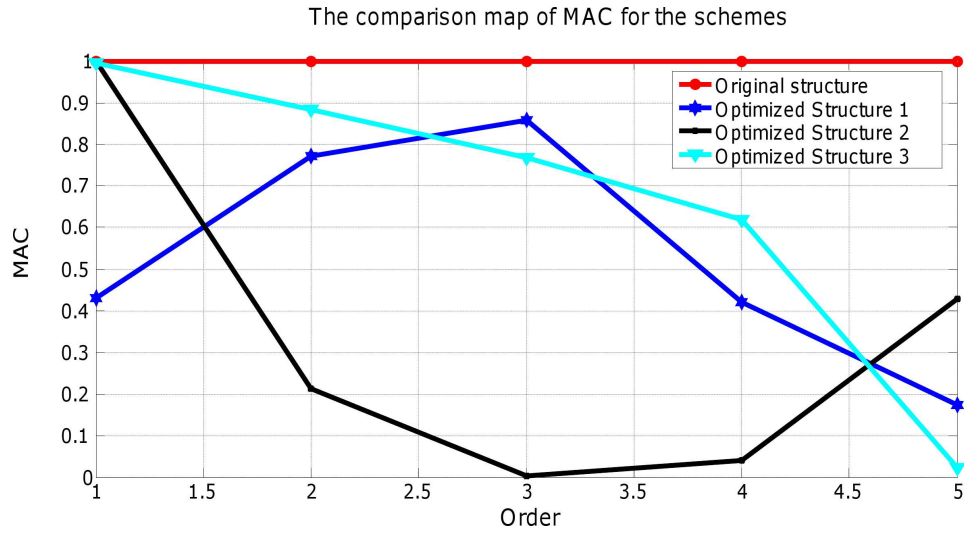


FIG. 11. Comparison map of MACs for the schemes.

into account, the first-order modal should be emphasized and, when considering this optimized structure 2 is obviously the best.

The response analysis of optimized structure 2 is conducted next and its polar diagram is presented in Fig. 12.

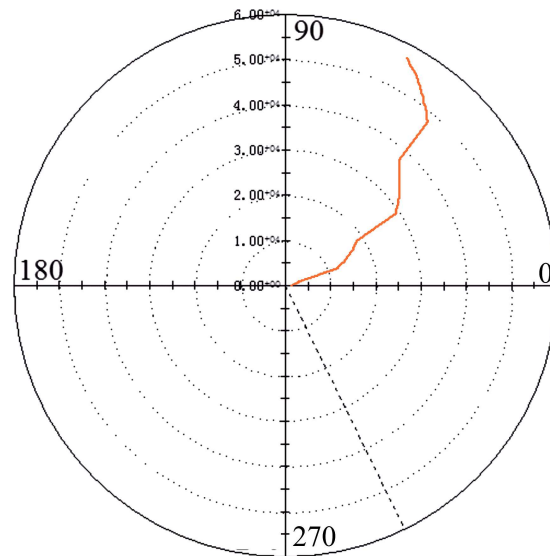


FIG. 12. Polar diagram response map of optimized structure 2.

From the diagram it can be seen that there are no mutational points like the ones shown in Fig. 8. The whole diagram is much smoother.

All things considered, optimized structure 2 is more suitable to be selected for the wing structure of a bionic flapping-wing aircraft than any of the other structures.

To draw such a conclusion, the authors assume that when compared to the original scheme and optimized structure 3, the truss added to optimized structure 2 makes the whole structure a triangle structure that is stable. Additionally, in optimized structure 1, two points are used as connection points between the flapping wings and the airframe, while structure 2 has only one point. In this case, on one hand, the flexibility of the transformation ability of the flexible wings can be better executed, giving a transmission gain to the craft's lift and on the other hand, the added truss can prevent the bending of the wings. When the wings intersect and transformation happens, the part changed is often far away from the airframe.

#### 4. MODAL TEST OF WING FLUTTER

In order to confirm the flutter situation of the optimized wing structure, a flutter test is conducted. Due to the changeable rigidity feature of the studied wing model, the hammering method is inappropriate. Instead, the stimulation method using an exciter is adopted. In terms of collecting data, the LMS SCADAS III modal analysis device and PCB acceleration sensor are used. The testing software is LMS Test. Lab 8B.

The stimulation signal of the exciter chooses the sine quick-scanned signal whose scanning cycle is shorter. Additionally, as the size of the flapping-wing is very small and the hinge joint surface between the wing and the driving

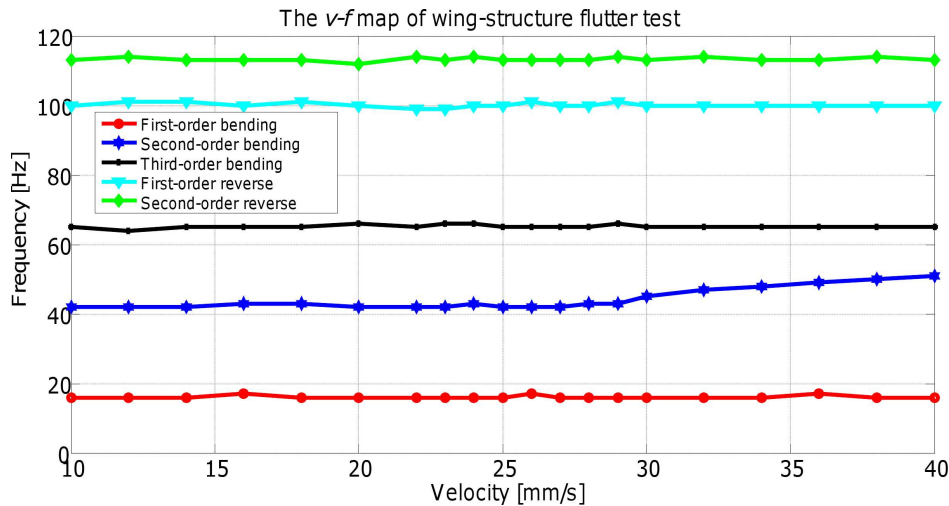


FIG. 13.  $v$ - $f$  map of wing-structure flutter test.

mechanism is relatively big, the supportive boundary model of joint interstice is adopted in order to increase the accuracy of the test.

On the basis of  $p-v$  method introduced in [16], the  $v-f$  map of wing flutter is obtained as shown in Fig. 13.

From Fig. 13, it can be concluded that the only flutter phenomenon occurs in the modal coupling of the second-order upward bending and the third-order bending. Beyond that, no more flutter phenomenon happens. As the coupling speed of second-order and third-order bending is faster than that of the flapping-wing aircraft, within the normal scope of scope, no flutter phenomenon will happen to the wings.

## 5. CONCLUSION

1. Through the finite element modal analysis of a bionic flapping-wing structure aircraft, its inherent frequency and vibration mode were obtained. This established the foundation for the upcoming optimized design with structural dynamic features, driving mechanism design and selection of electric machine parameter.
2. The vibration mode of the initially designed bionic flapping-wing aircraft vibration changes and intersects up and down when the resonance occurs, and after the wing membrane is covered, mutational shapes will easily emerge, which are bad for the stability of flight. To solve this problem, the wing structure was redesigned. The inherent frequency in the redesigned structure 2 was increased. Consequently, the wing structure did not obviously intersect up and down or bend, and the torsion vibration mode did not occur either. Therefore, this change in vibration mode was more suitable to bring transmission to the lifting force and keep it stable.
3. A flutter test was conducted in order to avoid the errors that might possibly exist in the theoretical calculation and design of the structure. The results of the test showed that within the flight speed scope of flapping wings, no flutter phenomenon or unstable movement would occur.

## ACKNOWLEDGMENT

This work is supported by Shanghai University of Engineering Science High Level Project to Cultivate Special (Grant Nos. 2012gp05) and the National Natural Science Foundation of China (NSFC) (Grant Nos. 51305254).

## REFERENCES

1. MAZAHERI K., EBRAHIMI A., *Experimental investigation of the effect of chordwise flexibility on the aerodynamics of flapping wings in hovering flight*, Journal of Fluids and Structures, **26**(4): 544–558, 2010.

2. MOUNTCASTLE A.M., DANIEL T.L., *Vortexlet models of flapping flexible wings show tuning for force production and control*, *Bioinspiration & Biomimetics*, **5**(4): 045005, 2010.
3. PELLETIER A., MUELLER T.J., *Low Reynolds number aerodynamics of low aspect-ratio, thin/flat/cambered-plate wings*, *Journal of Aircraft*, **37**(5): 825–832, 2000.
4. TIEN VAN TRUONG, JIHOON KIM, MIN JUN KIM, *et al.*, *Flow structures around a flapping-wing considering ground effect*, *Experiments in Fluids*, **54**(7): 1575–1594, 2013.
5. GENG-FENG Z., SHUN-FENG M., JI-GANG S., *et al.*, *High precision test method for dynamic imaging of space camera* [in Chinese], 2nd IEEE International Conference on Advanced Computer Control, **1**: 111–116, 2010.
6. YOUNG J., WALKER S.M., TAYLOR G.K., THOMAS A.L.R., *Numerical simulation of the aerodynamics of a desert locust (*Schistocerca gregaria*) in forward flight*, *Comparative Biochemistry and Physiology. A. Molecular & Integrative Physiology*, Elsevier Science Inc., **150**(3, Supplement): S79–S79, 2008.
7. WENYUAN C., WEIPING Z., *Flapping wing micro aircraft* [in Chinese], Shanghai, Shanghai Jiaotong University Press, 2010.
8. YAHUI Z., JIAHAO L., *Basics of structural dynamics* [in Chinese], Dalian University of Technology Press, Dalian, 2007.
9. QING W., BIN X., JIAQI H., *Optimized design of structural dynamic boundary condition based on topology optimization* [in Chinese], *Mechanical Science and Technology*, **31**(11): 1845–1850, 2012.
10. XUCHENG W., *Finite element method* [in Chinese], Tsinghua University Press, Beijing, 2003.
11. DECAN Z., *Several key problems of flapping-wing MAV* [in Chinese], Shanghai Jiaotong University, Shanghai, 2007.
12. IVANYI A., IVANYI P., IVANYI M.M., IVANYI M., *Hysteresis in structural dynamics*, *Physica B: Condensed Matter*, **407**(9): 1412–1414, 2012.
13. LALIBERTÉ J.F., KRAEMER K.L., DAWSON J.W., MIYATA D., *Design and manufacturing of biologically inspired micro aerial vehicle wings using rapid prototyping*, *International Journal of Micro Air Vehicles*, **5**(1): 15–38, 2013.
14. YUEFEI G., *Optimization design of boundaries and engineering implementation methods of structural dynamics* [in Chinese], Northwestern Polytechnical University, Xi 'an, 2005.
15. BO-LAN J., YUN-JU Y., XU B., *Topology optimal design of structural dynamic boundary condition based on ICM criterion method* [in Chinese], *Journal of Vibration Engineering*, **26**(1): 55–59, 2013.
16. XIE C., WU Z., YANG C., *Aeroelastic analysis of flexible large aspect ratio wing* [in Chinese], *Journal of Beijing University of Aeronautics and Astronautics*, **29**(12): 1087–1090, 2003.

*Received August 15, 2015; accepted version November 24, 2015.*

---